Yassin, A.; Trunk, M.; Czerny, F.; Fayon, P.; Trewin, A.; Schmidt, J.; Thomas, A.

Structure-Thermodynamic-Property Relationships in Cyanovinyl-Based Microporous Polymer Networks for the Future Design of Advanced Carbon Capture Materials

Journal article | Accepted manuscript (Postprint)
This version is available at https://doi.org/10.14279/depositonce-8352

This is the peer reviewed version of the following article:

Yassin, A., Trunk, M., Czerny, F., Fayon, P., Trewin, A., Schmidt, J., & Thomas, A. (2017). Structure-Thermodynamic-Property Relationships in Cyanovinyl-Based Microporous Polymer Networks for the Future Design of Advanced Carbon Capture Materials. Advanced Functional Materials, 27(26), 1700233. https://doi.org/10.1002/adfm.201700233,

which has been published in final form at https://doi.org/10.1002/adfm.201700233. This article may be used for non-commercial purposes in accordance with Wiley Terms and Conditions for Use of Self-Archived Versions.

Terms of Use
Copyright applies. A non-exclusive, non-transferable and limited right to use is granted. This document is intended solely for personal, non-commercial use.

WISSEN IM ZENTRUM UNIVERSITÄTSBIBLIOTHEK

Technische Universität Berlin

Structure–Thermodynamic-Property Relationships in Cyanovinyl-Based Microporous Polymer Networks for the Future Design of Advanced Carbon Capture Materials

Ali Yassin, Matthias Trunk, Frank Czerny, Pierre Fayon, Abbie Trewin, Johannes Schmidt, and Arne Thomas**

Nitrogen-rich solid absorbents, which have been immensely tested for carbon dioxide capture, seem until this date to be without decisive molecular engineering or design rules. Here, a family of cyanovinylene-based microporous polymers synthesized under metal-catalyzed conditions is reported as a promising candidate for advanced carbon capture materials. These networks reveal that isosteric heats of CO_2 adsorption are directly proportional to the amount of their functional group. Motivated by this finding, polymers produced under base-catalyzed conditions with tailored quantities of cyanovinyl content confirm the systematical tuning of their sorption enthalpies to reach 40 kJ mol^{-1}. This value is among the highest reported to date in carbonaceous networks undergoing physisorption. A six-point-plot reveals that the structure–thermodynamic-property relationship is linearly proportional and can thus be perfectly fitted to tailor-made values prior to experimental measurements. Dynamic simulations show a bowl-shaped region within which CO_2 is able to sit and interact with its conjugated surrounding, while theoretical calculations confirm the increase of binding sites with the increase of Ph-C=C(CN)-Ph functionality in a network. This concept presents a distinct method for the future design of carbon dioxide capturing materials.

1 Introduction

As concluded from the recent scenarios developed by British Petroleum and the International Energy Agency, fossil fuel demands will continue to grow in the near future.[1] This is further driven by the discovery of new and emerging unconventional sources, such as tight oil and shale gas, which are becoming more technically accessible.[2] Meanwhile, continued CO_2 emissions have been associated with rising sea levels, ocean acidification, increased droughts, reductions in crop productivity, and deaths due to infectious diseases.[3] Still, it is predicted in addressing the problem of global climate change, that a cigarette-like addiction for fossil fuel usage may generate a long period of time in which people express sincere desire to convert to clean energy resources but accomplish little to achieve it.[4] Until a zero carbon footprint could be reached, it seems of urgent priority now to bring foreword new materials that would serve under the technical processes developed for CO_2 capture.

One such process is the postcombustion capture from flue gas, a predominantly CO_2/N_2 gas separation at relatively low pressures, which has been the most explored strategy to date since it

could be readily retrofitted to existing power plants.[5] However, due to stability and selectivity concerns in addition to the large amounts of energy required for their regeneration, through different swing adsorption techniques, even the best carbon-capture materials nowadays are unfeasible for large-scale deployment.[6] Originally, contributions in the field were meant to overcome the sequestration energy penalty of wet scrubbing methods, involving alkanolamines, and lead to the introduction of solid adsorbents, in particular porous ones, as potential solution to the problem. Zeolites, silica, activated carbons, metal-organic frameworks,[7] and lately tailor made covalent organic frameworks for carbon dioxide capture[8] had become under intensive consideration, while microporous polymer networks (MPNs) were much recently introduced as well.

MPNs attracted much attention due to their unique feature of combining high accessible surface areas with a wide range of functional groups while preserving chemical robustness and thermal stability, albeit in exchange of superior crystallinity.[9] Cooper and co-workers undertook sincere effort in investigating different MPNs for CO_2 capture and studied the effects of surface area,[10] water coadsorption,[11] and chemical functionality[12] in several conjugated networks (CMPs). Zhou and co-workers presented breakthrough uptakes of CO_2 by postfunctionalizing PPN-6 based materials with polyamines and sulfonates.[13] Yavuz and co-workers also showed much attention for carbon capture and introduced different novel MPNs with attractive properties and tuned enthalpies.[14] While considerable work is being conducted to investigate more advanced polymers for such applications, recognized by the escalation of reports in the literature,[15] the engineering rules for their molecular design seem without solid bases. It has been stated that tuning the thermodynamics of interaction between CO_2 and the adsorbent is one of the most crucial considerations in improving the energy efficiency of CO_2 capture.[16] Isosteric heats of adsorption were certainly modified, for example by changing the nature of incorporated functional group,[12,17] but the term “fine tuning” has been mistakenly, or probably too optimistically, used in literature only to describe diverse experimental values and qualitative changes in heats of adsorptions. To the best of our knowledge indisputable tuning of enthalpy to precise tailor-made quantities was heretofore out of reach.

2 Experimental Results and Discussion

Here, we describe the synthesis, characterization, and experimental gas sorption properties of a series of engineered MPNs produced under both metal-catalyzed and metal-free reaction conditions and demonstrate a prime example in which CO_2 enthalpies can be well tailored to definite values via manipulating the corresponding content of cyanovinylene bridges. Theoretical models of the amorphous polymers were generated and their structures and porosities were assessed, while binding sites of carbon dioxide in these networks and their diffusion in the different cyanovinyl-based polymers were sampled by performing molecular dynamics simulations.

Although nitrogen-rich materials were immensely tested due to their high selectivities, still, the cyanovinyl linkage has not yet been investigated for carbon capture. Beyond such reason, our interest stems from the fact that this moiety could be generated via a green synthetic route through simple condensation reactions, in which water is the sole by-product.[18]

2.1 Networks P1–P4 Based on (Benzene-1,3,5-Triyl) Tris(2-Phenylacrylonitrile)

2.1.1 Synthesis of the Metal-Catalyzed Polymers under Optimized Conditions for Efficient Coupling

Since at first we wanted to investigate metal-catalyzed polymer networks, the tris-iodinated derivative of (benzene-1,3,5-triyl)tris(2-phenylacrylonitrile), monomer 1 (**Figure 1**), was prepared in near-quantitative yields from commercially available compounds (Section S1, Supporting Information). Obtained single

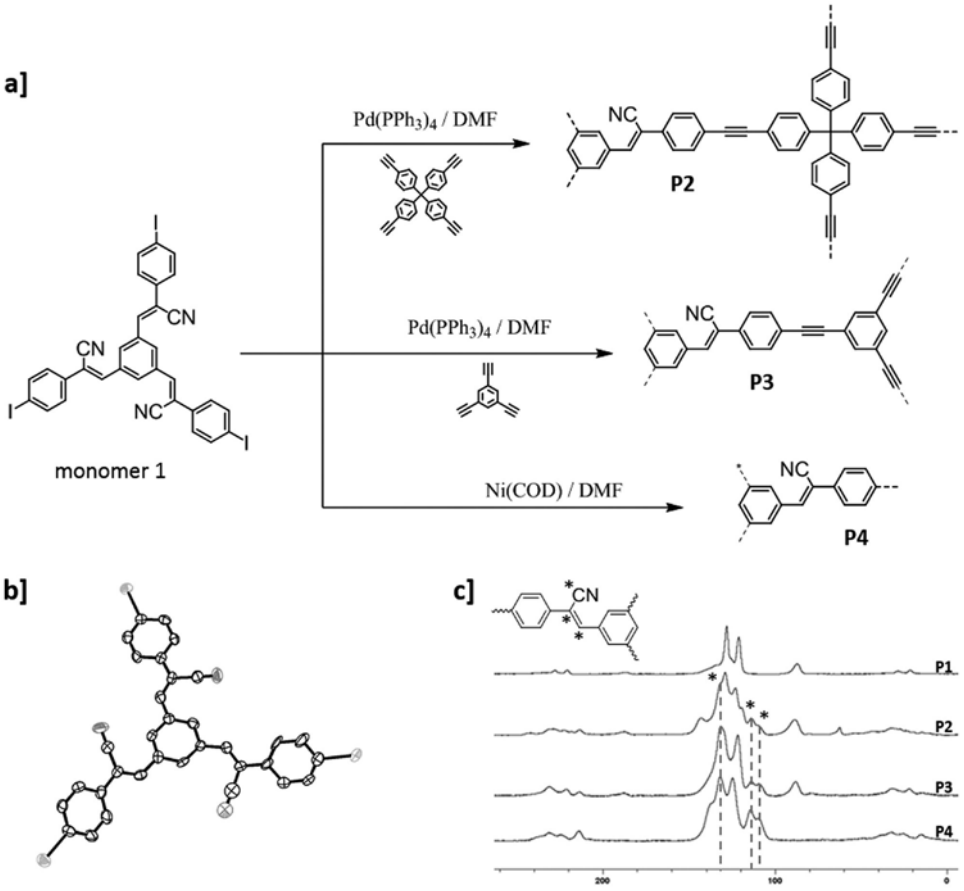

Figure 1. a) Metal-catalyzed reactions of monomer 1 under different conditions for MPNs **P2**, **P3**, and **P4**. b) Single crystal X-ray resolved structure of the monomer. c) ^{13}C solid state NMR of the MPNs showing the chemical shifts corresponding to the cyanovinyl moiety, and their absence in **P1**.

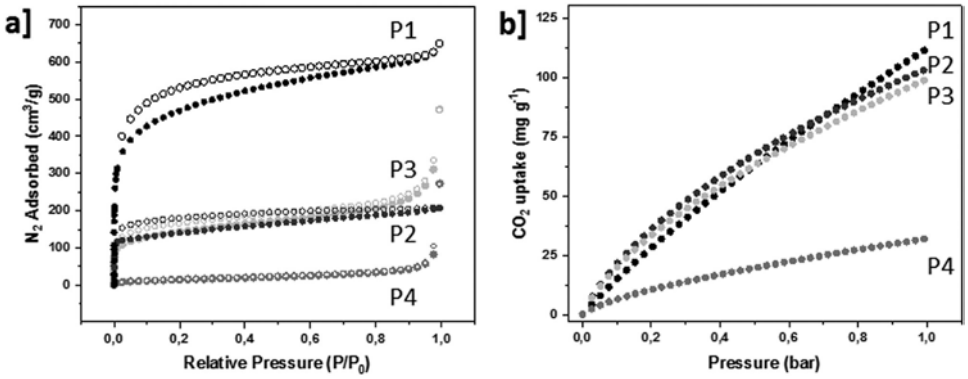

Figure 2. a) N_2 adsorption (solid) and desorption (hollow) isotherms of the metal-catalyzed networks at 77 K; b) CO_2 uptakes at 273 K.

crystals reveal through X-ray diffraction that phenyl rings adopt a *trans* confirmation relative to one another in a monoclinic crystal system (Figure 1b, and Section S11 and crystallographic data, Supporting Information). The monomer was later used as tecton to generate three different metal-catalyzed MPNs under optimized conditions; by coupling with tetrakis(4-ethynylphenyl) methane or 1,3,5-triethynylbenzene in a Sonogashira–Hagihara reaction, with Pd, to produce **P2** and **P3**, respectively and by direct polymerization via Yamamoto coupling,[19] with Ni, to produce **P4** (Figure 1a and Section S1, Supporting Information). As follows, the obtained networks have different weight percentages (wt%) of cyanovinylene content (precised in Section S2, Supporting Information). Poly(aryleneethynylene) network **P1** was prepared as unfunctionalized reference polymer free of cyanovinylene bridges. Under optimized synthetic conditions recently developed by our group,[20] triple bonds in **P1** are completely coupled excluding any homo-polymerization seen in previous reports.[21]

The obtained polymers, amorphous as concluded from powder (X-ray diffraction) XRD analysis (Section S3, Supporting Information), were initially characterized with solid-state ^{13}C NMR confirming the three corresponding cyanovinyl chemical shifts at 108, 114, and 132 ppm in the functionalized polymers; **P2**, **P3**, and **P4** (Figure 1c and Section S4, Supporting Information). Further investigations by Fourier transform infrared (FTIR) spectroscopy also showed the characteristic –CN stretching at ≈2220 cm^{-1} (Section S5, Supporting Information). In both techniques these signals were absent for **P1** as eventually expected.

2.1.2 Nitrogen Sorption Properties of the MPNs **P1–P4** and their Carbon Uptake

The porosity of networks was analyzed by collecting nitrogen sorption measurements on activated samples at 77 K revealing type I isotherms (**Figure 2**a) with Brunauer–Emmett–Teller (BET) surface areas exceeding 500 $m^2 g^{-1}$ for **P2** and **P3**. The largest quantities of N_2 uptake were observed at low relativepressures indicative of adsorption into micro pores which is reflected in the pore size distribution calculated from their isotherms (Section S7, Supporting Information). While CMP-1 is already known to be a very porous material, **P1** consistently reaches a BET surface area of 1700 $m^2 g^{-1}$ explaining its high carbon dioxide uptake at 273 K (Figure 2b). Measurements were also recorded at 298 K to calculate the isosteric heats of adsorption (Q_{st}) from dual-site Langmuir fits of the CO_2 isotherms. Likewise they were performed with N_2 to determine the networks' selectivities under flue-gas conditions (85:15/N_2:CO_2) with single-gas isotherms (Section S8, Supporting Information) using the ideal adsorbed solution theory model.[22]

Table 1 depicts a table summarizing the gas sorption properties of the networks under different experimental conditions. **P1**, **P2**, and **P3** show impressive CO_2 capture values exceeding 100 mg g^{-1} at 273 K and decreasing by around 40% at higher temperature. A nitrile containing polymer structurally similar to **P2** was reported by Thirion et al. with BET surface area of 650 m^2 g^{-1} and interestingly similar CO_2 uptake near 100 mg g^{-1}.[23] The capture of carbon in **P1** comes mostly from its high porosity, which clearly relates the uptake in the other networks to their cyanovinyl content, making the latter a very interesting building block for carbon capture. Even for **P4**, which consists only of cyanostilbene units that are not entirely linear but rather more flexible and could relax into a nonporous condensed state,[24] the functional group maintains the polymer with an uptake of 32 mg of CO_2 per 1 g of material. It is noted however that selectivities of these networks over N_2 were relatively poor. In analyzing the measured isosteric heats of adsorption we discovered a close-to-perfect linear correlation with reference to the corresponding percentages of functional group (Table 1, bold values and Section S9, Supporting Information). This was inspired by similar well-studied relationships in π-conjugated systems which show strong dependence between structure and

Table 1. Gas sorption properties of the metal-catalyzed polymers.

Network	S_{BET} [m^2 g^1]	Pore width [nm]	CO_2 uptake[a] [mg g^{-1}]		Selectivity[b] CO_2/N_2	Q_{st} [kJ mol^{-1}]	Functional group [wt%]
			273 K	298 K			
P1	1700	1.35	111	59	Ref. [14]	**20.9**	**0**
P2	520	0.85	103	58	15	**28.2**	**19.7**
P3	510	1.45	99	53	11	**30.2**	**25.4**
P4	60	1.47	32	19	19	**32.5**	**33.5**

a)Uptakes at 1 bar; b)Selectivities at flue gas conditions (85:15/N2:CO2). wt% represents the percentage of C3H1N per repeating unit of polymer (see Section S2 in the Supporting Information).

the corresponding electronic property for example.[25] The relation obtained, Q_{st} = 21.07 + 0.37(wt%), predicts for instance, that a 45 wt% of incorporated functionality will result in a sorption enthalpy of 38 kJ mol^{-1}. This could be even tuned to values as high as 40 kJ mol^{-1} if the weight content is increased to 50%.

2.2 Networks P5 and P6 Based on (Benzene-1,3,5-Triyl) Triacetonitrile

2.2.1 Synthesis of the Base-Catalyzed Polymers under Metal-Free Reaction Conditions and their Gas Sorption Properties

To further investigate this unprecedented structure– thermodynamic-property relationship we designed another set of MPNs under metal-free conditions this time, where monomer

2 (benzene-1,3,5-triyl)triacetonitrile (Section S1, Supporting Information) was condensed with commercially available terephthalaldehyde or benzene-1,3,5-tricarbaldehyde, in presence of a base, to produce **P5** and **P6**, respectively. The only by-product of such polymerization is water (**Figure 3**a). The percentage of cyanovinylene bridges in these polymers are engineered to the definite values previously discussed, while solid state ^{13}C NMR and FT-IR confirmed the corresponding structures (Sections S3 and S4, Supporting Information).

Gas sorption measurements for **P5** and **P6** were collected under the same conditions of the previous networks (**Table 2**). Nitrogen isotherms show BET surface areas around 100 $m^2 g^{-1}$ (Section S7, Supporting Information) which is expected in such relatively flexible systems, but captured CO_2 quantities still reach values of 90 mg g^{-1}. Indeed it has already been observed that BET surface areas do not directly dominate the carbon capture in polymer networks at low pressures.[10] The uptake was accompanied by a huge seven- to ninefold increase of selectivities over nitrogen gas reaching values close to 100 for **P6** (Section S10, Supporting Information). Figure S9 (Supporting Information) shows the measured isosteric heats of adsorption from the CO_2 isotherms collected at 273 and 298 K. The important contribution of the obtained data (Table 2, bold values) confirms the discussed relation earlier. Indeed sorption enthalpies of **P5** (with 44.7 wt% functional group) and **P6** (with 50.5 wt%) show the predicted values at ≈38 and 40 kJ mol^{-1}, respectively, as expected. **P6** has one of the highest enthalpies reported to date in carbonaceous physisorbents for CO_2; the next upper values in literature being related to direct chemisorption.[26] Plotting the enthalpy values of all the different networks (**P1**–**P6**) as function of the cyanovinyl content reveals an excellent matching with the best-fitting line in Figure 3c. Noteworthy this relation holds true for polymers prepared under several reaction conditions that are entirely different, as illustrated earlier (Section S9, Supporting Information).

2.2.2 Vacuum Swing Adsorption (VSA) and Temperature- Programmed Desorption Analysis (TPD) of the Polymers P1–P6

The energy penalty suffered during the regeneration step of materials used for carbon capture is usually associated with their high affinity to CO_2 as the adsorption process is mostly of chemical nature and involves bond formations that are hard

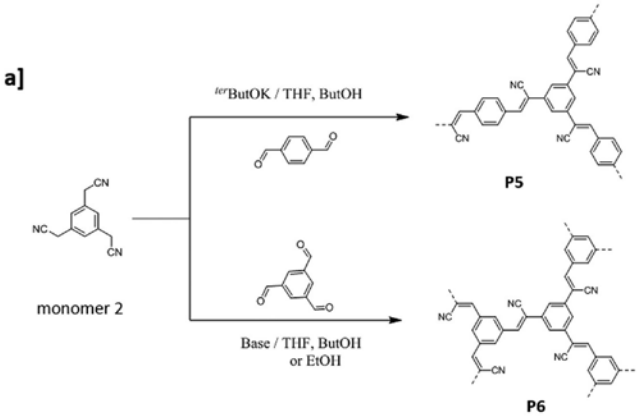

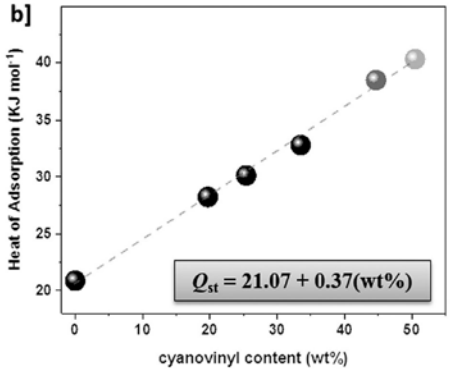

Figure 3. a) Metal-free condensation under basic conditions for **P5** (dark grey) and **P6** (light grey). b) The linear relationship between Q_{st} and the wt% of cyanovinyl content in the networks. The best fitting line is dashed. **P5** (pink) and **P6** (dark yellow).

to break. We were able, through the presented concept, to generate networks with their highest enthalpy values tuned just below the chemisorption barrier (45–55 kJ mol^{-1}) at which the regeneration is expected to require minimal energy. To test this, network **P6** (40 kJ mol^{-1}) was cycled under conditions similar to VSA with an autosorb iQ2 automated analyzer. In every cycle the material was saturated with CO_2 up to 1 bar at room temperature. Desorption was followed by applying under pressure, without any thermal heating, for an automated period of time during which the analyzer relaxes to some stable pressure. In average 4 min at 1 mbar and ambient temperature were enough for the complete desorption and regeneration of the material (**Figure 4**a, starting point of every isotherm). In addition, after 10 cycles there was not any apparent loss in uptake capacity, thus indicating the high stability and cyclability of this network (Figure 4a, end point of every isotherm).

Table 2. Gas sorption properties of the base-catalyzed polymers.

Network	S_{BET} [m^2 g^1]	CO_2 uptake [mg g^{-1}]	Selectivity O_2/N_2	Q_{st} [kJ mol^{-1}]	Functional group [wt%]
P5	80	59	74	**38.5**	**44.7**
P6	112	90	96	**40.3**	**50.5**

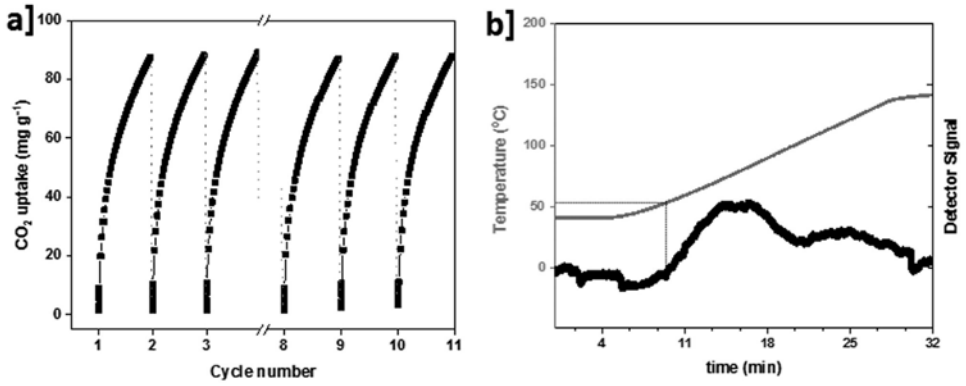

Figure 4. a) CO_2 isotherms for **P6** at 273 K and 1 bar, the material being cycled 10 times. Each regeneration step takes an average of 4 min at 1 mbar. b) TPD plot for **P6**. In grey is denoted the temperature ramp profile used for desorption. The signal for CO_2 is given by the black curve.

To further investigate the physisorptive nature of CO_2, TPD was performed on saturated samples with CO_2 at 1 bar.[27] Helium was used as carrier gas and the material was heated to elevated temperatures for the full evacuation of the host. TPD shows that gas release starts slightly above 50 °C while most of the CO_2 is already desorbed before 80 °C (Figure 4b). The enthalpy values of the networks, in addition to their straightforward regeneration under simple conditions, as demonstrated by the techniques, prove the physisorption character of CO_2 and contribute to their

interest as being a cornerstone for designing new materials of higher surface areas with enhanced carbon uptakes while keeping this easy regeneration feature.

3 Dynamic Simulations and the Generation of Network Models

Generation of amorphous networks is challenging due to the lack of experimental data to aid the construction of a representative model. Furthermore, the generation process is often limited to small cells that do not allow for modeling of the nanoscale structure of the porous polymers which could have an influence on the final properties.

3.1 Construction of P1–P6 Network Models

Here, we use an automated structure generation methodology for the cyanovinyl-based extended network materials that exploits GPU hardware for increased speed and size of simulation. This methodology is implemented in the *Ambuild* code that integrates with HOOMD-blue and DL_POLY molecular dynamic simulation codes.[28] For each poly mer we seed an initial simulation cell with stoichiometric quantities of the respective building blocks and solvent molecules. We designate end group atoms and cap atoms, together with a number of structural and geometric rules that build the network in a chemically realistic manner (**Figure 5**, Structures C1–D3).

For **P1**, we define the building blocks as 1,4,-diiodobenzene C1 and 1,3,5-triethynylbenzene D1 monomers with the cap atoms, respectively, phenyl-I and ethynyl-H, being removed once a bond is formed between the respective phenyl-C and ethynyl-C end group atoms. Similarly, for **P2**–**P4** the common building block is defined as C2 (monomer 1), with the cap atom defined as the phenyl-I and the bonded phenyl-C as the end group. **P2** is constructed from C2 and D2, **P3** is constructed from C2 and D1, and **P4** is constructed from C2 alone. For **P5** and **P6** the monomer units are not used as the chemistry is challenging to mimic the building procedure, rather we define two further building units based on the resulting frameworks and monomer units; C3 based upon monomer 2, and D3

(1,3,5-triiodophenyl) based upon benzene-1,3,5-tricarbaldehyde. Thus, **P5** is constructed from C3 and C1 and **P6** is constructed

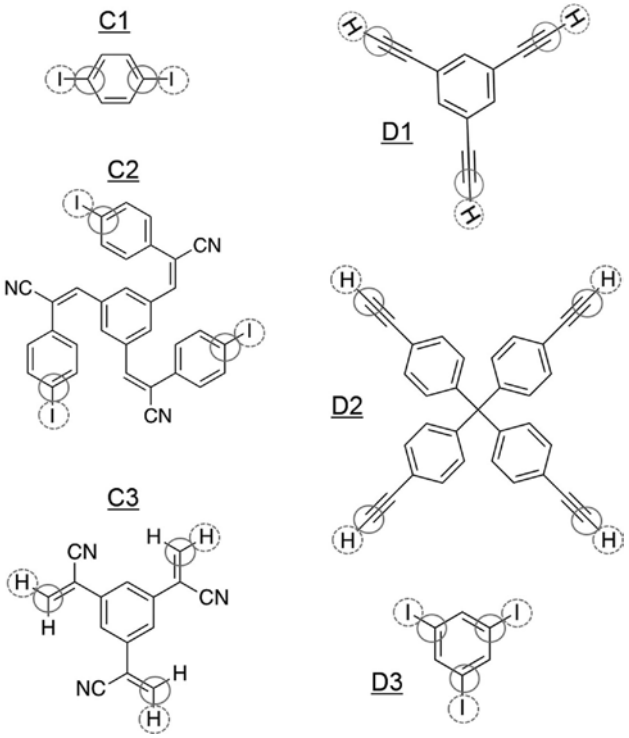

Figure 5. Structures optimized using DFT as building blocks for the construction of the network models. Atoms with a hashed circle are the designated cap atoms, and those with a solid circle are the end groups.

Table 3. The building block ratios for the respective polymer model systems.

Polymer	Building block 1	Building block 2	Ratio	Solvent
P1	C1	D1	3:2	DMF
P2	C2	D2	4:3	DMF
P3	C2	D1	1:1	DMF
P4	C2	–	–	DMF
P5	C3	C1	2:3	THF/BuOH (1:1)
P6	C3	D3	1:1	THF/BuOH (1:1)

from C3 and D3 (**Table 3**; Figure 5). In all cases bonding is tested between the respective cap atoms which are removed once a new bond is formed at the end groups based upon the geometrical and structural rules. For **P5** and **P6**, any cap atom or functionality that remains at the end of the network's generation procedure is replaced with the respective terminal group expected for the synthetic procedure.

A number of molecular dynamic (MD) simulation loops are undertaken with structural sampling for potential bond formation. Upon bond formation, the structure undergoes a full, rigid-body geometry optimization before returning to the MD loops. The full building procedure is reported (Section S12 and Table S2, Supporting Information).

3.2 Structure and Porosity Assessment of the Cyanovinyl-Based MPN Models

Here, we target network densities of 0.7–1.1 g cm^{-3} as this range is commonly determined for similar CMP materials with similar porosity data. CMP materials with high surface areas tend to have low densities. The networks are generated in presence of solvent to get the target density then "de-solvated" by removal of the solvent and further molecular dynamic and geometry optimization steps are undertaken to obtain the final network structures. **P1–P3** have densities between 0.76 and 0.81 g cm^{-3} obtained (Section S14, Supporting Information), consistent with other CMP materials with similar surface area and porosity uptake properties where the experimental density has been determined.[29] **P4** has a density of 0.76 g cm^{-3}, lower than expected given the relatively low surface area obtained experimentally. **P5** and **P6** have densities of 1.02 and 1.4 g cm^{-3}, respectively, consistent with the low surface areas obtained experimentally. We believe that the increased density reflects the increased flexibility of the network formed and its ability to pack efficiently.

Comparison of elemental analysis of the generated network materials to the experimental data shows the same trend of the weight percentage of carbon decreasing and a weight percentage of nitrogen increasing going from **P1** to **P6** (Table S3, Supporting Information).

Geometric surface areas were calculated for each model and are shown in Table S4 in the Supporting Information. The trend is in broad agreement with that obtained experimentally with surface areas decreasing from **P1** to **P6**. Calculated pore size distributions are shown in Section S15 in the Supporting Information. For **P1–P4** they range between 5 and 18 Å, broadly centered around 10–12 Å, in agreement with the ranges observed experimentally. **P5** and **P6** have pore sizes ranging between 5 and 10 Å, reflecting the increased density and efficient packing of the network. The experimental pore size distribution for all polymers shows the presence of mesopores with pore widths greater than 30 Å. It is not possible to take account of these larger pores as the unit cell size artificially restricts the pore width to the microporous region (Figure S13, Supporting Information).

3.3 Carbon Dioxide Binding Sites in Cyanovinyl-Based MPNs Models

The binding energy of CO_2 to functional groups within the polymer network was assessed through density functional theory calculations with basis set superposition error (BSSE) correction. A fragment of the **P5** and **P6** polymer was generated as a representative structure for the CN rich functionality of each polymer. The binding energy of the CO_2 molecule was calculated for a number of positions. A similar high energy binding site for **P5** and **P6** was found where the CO_2 is able to interact with a CN, C=C, and a phenyl ring with a binding energy of 23.35 and 21.13 kJ mol^{-1}, respectively. Interestingly, the binding site forms a bowl shaped region within which the CO_2 is able to sit and interact with the conjugated functionality surrounding it. Adding a further fragment of the respective polymer results in a high energy-binding site surrounded by an additional bowl shaped region and the CO_2 is therefore able to interact with further conjugated functionality. This leads to an increased binding energy of 34.14 and 35.44 kJ mol^{-1} for **P5** and **P6**, respectively. A further fragment of the respective polymer is added to the existing binding site leading to binding energies of 45.86 and 42.97 kJ mol^{-1} (Section S16 and Tables S5–S10, Supporting Information). In conclusion, as the

concentration of CN and associated C=C functionality increases so does the number of available high energy binding sites. This is in excellent agreement with the trend in isosteric heat of adsorption obtained experimentally for **P1** through to **P6**.

Assessment of the high energy binding sites with three polymer fragments reveals that the N atoms of the CN functionality are located between 3 and 9 Å apart with most being at ≈7.5 Å distance apart.

To assess the distribution of nitrile groups within the generated networks we performed a radial distribution analysis on the nitrogen atoms of the nitrile groups. **Figure 6**a shows the comparison of this distribution in the different polymer systems. All polymers show a peak at N–N distance of 3–5 Å reflecting the nitrogen–nitrogen distance of the nitrile groups within the respective C2 and C3 repeating units. Another peak at 8.5 Å is common to all the polymers representing the N–N distance between nearest neighbor C2 or C3 groups. **P2** has the sharp peaks in the radial distribution reflecting the relatively rigid nature of the network resulting in well-defined distances between neighboring nitrile groups. The peaks become progressively broader going from **P3** to **P6** reflecting the range of distances available due to the flexibility of the network. For **P4**, **P5**, and **P6**, the peak is shifted to lower values with **P5**

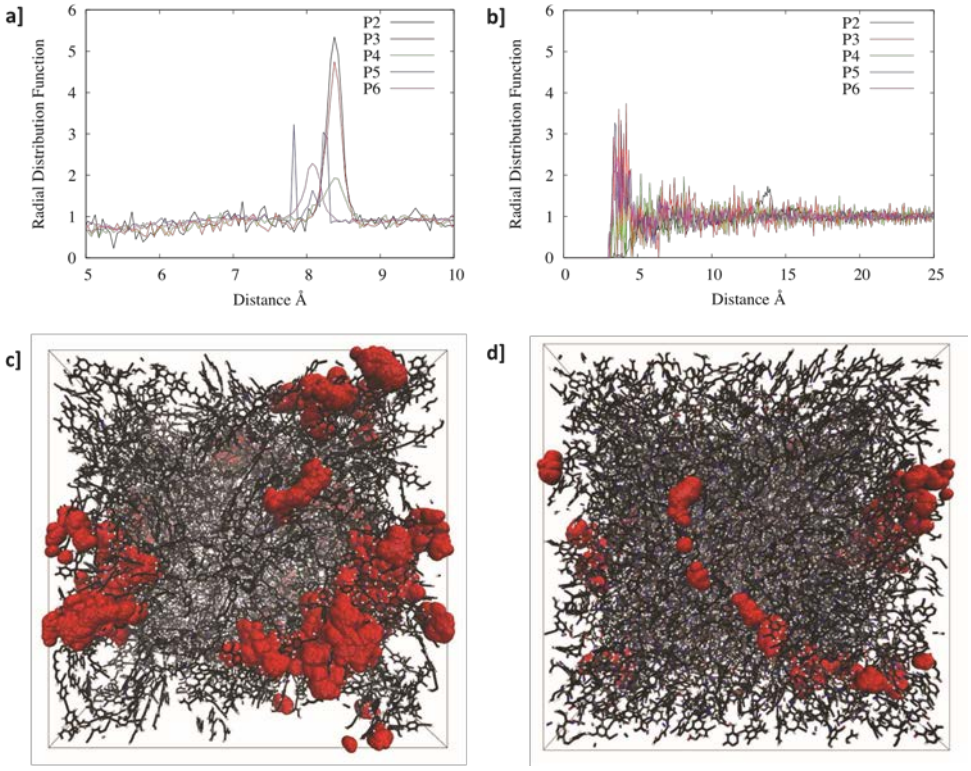

Figure 6. a) Comparison of the radial distribution of N in the polymers; b) comparison of the radial distribution of the C atom, in CO_2, to the N of the polymers; c) overlay of CO_2 diffusion in **P2**; and d) CO_2 diffusion in **P6**.

having an additional peak at 7.8 Å (Section S17, Supporting Information). This reflects the increasing concentration of CN functionality and the formation of additional high-energy CO_2 binding sites as described above.

3.4 Carbon Dioxide Binding

CO_2 can occupy a number of different sites within the pore structure and may be able to interact with multiple nitrile groups. To sample the sorption sites and their respective proximity to network nitrile groups we seed 10 CO_2 molecules within each network, we then perform molecular dynamics simulations and optimization sampling the radial distribution function of the central carbon atom of the CO_2 molecules to the nitrogen atom of the network nitrile groups. The resulting radial distribution plots are shown in Section S18 (Supporting Information).

The plots show that the CO_2 molecule for all systems is able to sample sites with a distance of 3.5 Å to the nitrile group (Figure 6b), the distance expected for the higher binding energy sites. For **P3**, **P4**, **P5**, and **P6** the CO_2 molecule is able to sample sites with a distance of 3.1 Å distance to a nitrile group. Furthermore, the number of times that sites of distance of 5 Å or less to a nitrile site, is greatly increased compared to **P2**.

To further assess the diffusion of CO_2, we perform molecular dynamic simulation of the diffusion of a molecule of CO_2 diffusing through **P6**. We describe the **P6** polymer as fully flexible with all bonds and angles being described fully meaning that the **P6** polymer is able to be flexible and dynamic. As a comparison we also perform the same diffusion experiment with **P2** (Figure 6c,d).

The CO_2 molecule is able to freely diffuse through **P2** as the pore structure is large and connected. The diffusion of the CO_2 molecule is more restricted in **P6** but the molecule is still able to diffuse through a large volume and sample multiple binding sites. The diffusion coefficients were calculated for each polymer. In **P2**, diffusion coefficients of 5.2 and 12.15 $nm^2\ ns^{-1}$ were calculated reflecting diffusion in a small pore and larger pore regions of the model, respectively (Figure S32, Supporting Information). In **P6**, a diffusion coefficient of 3.08 $nm^2\ ns^{-1}$ was calculated (Figure S33, Supporting Information). The diffusion of the CO_2 in **P6** is slower as the system has only small pore regions with pore diameters less than 10 Å. Closer inspection of the CO_2 diffusion trajectory in **P6** shows that the mole cule pathway is through pores that are surrounded by the conjugated functionality and we would hence expect that these pathways will have high energy binding sites.

4 Conclusion

In conclusion, we have successfully tuned the sorption enthalpies of carbon dioxide in amorphous polymer networks for tailor-made values by controlling the weight percentage of cyanovinylene content. Accordingly, we designed and synthesized microporous polymers under different poly merization methods with engineered percentages of functional groups as interesting materials for carbon capture. While the networks achieved CO_2 uptakes higher than 100 mg g^{-1}, an unprecedented structure–thermodynamic-property relationship was revealed as the isosteric heats of adsorption proved to be linearly proportional to the content of the cyanovinyl group. In consequence, enthalpies were adjusted to tailor-made values by designing new polymers with the required amount of cyanovinyl bridges. An environmentally friendly metalfree condensation reaction from cheap starting materials, and only water as by-product, generated porous polymers with CO_2 sorption enthalpies as high as 40 kJ mol^{-1}, among the highest reported to date for physisorption in MPNs and exhibiting exceptional selectivities close to 100. TPD measurements and VSA technique confirmed the physisorptive nature of the interaction while regeneration of the polymer was achieved at slight under pressure and ambient temperature, or at 80 °C and under normal pressure. Thorough theoretical calculations and dynamic simulations of the amorphous polymers showed that the

binding sites form a bowl shaped region for CO_2 adsorption and that these sites increase with the concentration of CN and associated C=C functionality in the networks.

Although these materials are not meant to be directly used for commercial application, the explored structure–property relationships in this study could draw the attention for new design rules of future polymers with advanced CO_2 capture properties. Moreover, their precisely controlled structures might give them high advantages as additives in mixed membranes for gas separation applications,[30] the issue we are currently developing with our materials.

5 Experimental Section

Experimental details including crystallography data, full synthetic procedures, FT-IR, elemental analysis and NMR spectra, powder XRD measurements, gas sorption properties, theoretical calculations, and dynamic simulations are available in the Supporting Information.

CCDC 1440645 contains the supplementary crystallographic data for this paper. These data can be obtained free of charge from The Cambridge Crystallographic Data Centre via www.ccdc.cam.ac.uk/data_request/cif.

Supporting Information

Supporting Information is available from the Wiley Online Library or from the author.

Acknowledgements

A.Y. and M.T. contributed equally to this work. A.Y. acknowledges funding from the European Research Council within the project 278593_ ORGZEO. The authors thank Elisabeth Irran for single crystal X-ray diffraction and Anton Sagaltchik of BasCat, the joint UniCat-BASF lab at TU Berlin, for assistance in TPD.

Conflict of Interest

The authors declare no conflict of interest.

Keywords

amorphous polymer modeling, carbon capture, cyanovinylene microporous polymers, sorption enthalpy, structure–property relationships

Received: January 14, 2017

Revised: February 25, 2017

Published online: May 29, 2017

[1] IEA: World Energy Outlook, BP Energy Outlook 2035, January 2014, Technical Report, **2015**.

[2] S. H. Mohr, J. Wang, G. Ellem, J. Ward, D. Giurco, *Fuel* **2015**, *141*, 120.

[3] Fourth Assessment Report of the Intergovernmental Panel on Climate Change, Summary for Policymakers, **2007**.

[4] S. Suranovic, *Global Environ. Change* **2013**, *23*, 598.

[5] M. Kanniche, R. Gros-Bonnivard, P. Jaud, J. Valle-Marcos, J.-M. Amann, C. Bouallou, *Appl. Therm. Eng.* **2010**, *30*, 53.

[6] C.-H. Yu, C.-H. Huang, C.-S. Tan, *Aerosol Air Qual. Res.* **2012**, *12*, 745.

[7] A. H. Lu, G. P. Hao, *Annu. Rep. Prog. Chem., Sect. A: Inorg. Chem.* **2013**, *109*, 484.

[8] a) N. Huang, X. Chen, R. Krishna, D. Jiang, *Angew. Chem. Int. Ed.* **2015**, *54*, 2986; b) N. Huang, R. Krishna, D. Jiang, *J. Am. Chem. Soc.* **2015**, *137*, 7079.

[9] a) A. Thomas. *Angew. Chem. Int. Ed.* **2010**, *49*, 8328; b) A. I. Cooper, *Adv. Mater.* **2009**, *21*, 1291; c) Y. Xu, S. Jin, H. Xu, A. Nagai, D. Jiang, *Chem. Soc. Rev.* **2013**, *42*, 8012.

[10] R. Dawson, E. Stockel, J. R. Holst, D. J. Adams, A. I. Cooper, *Energy Environ. Sci.* **2011**, *4*, 4239.

[11] R. Dawson, L. Stevens, T. Drage, C. Snape, M. Smith, D. J. Adams, A. I. Cooper, *J. Am. Chem. Soc.* **2012**, *134*, 10741.

[12] R. Dawson, D. J. Adams, A. I. Cooper, *Chem. Sci.* **2011**, *2*, 1173.

[13] a) W. Lu, J. Sculley, D. Yuan, R. Krishna, Z. Wei, H. C. Zhou, *Angew. Chem. Int. Ed.* **2012**, *51*, 7480; b) W. Lu, W. Verdegaal, j. Yu, P. Balbuena, H. K. Jeong, H. C. Zhou, *Energy Environ. Sci.* **2013**, *6*, 3559.

[14] a) H. Patel, F. Karadas, J. Byun, J. Park, E. Deniz, A. Canlier,

Y. Jung, M. Atilhan, C. T. Yavuz, *Adv. Funct. Mater.* **2013**, *23*, 2270; b) D. Ko, H. Patela, C. T. Yavuz, *Chem. Commun.* **2015**, *51*, 2915;

c) D. Thirion, V. Rozyyev, J. Park, J. Byun, Y. Jung, M. Atilhan, C. T. Yavuz, *Phys. Chem. Chem. Phys.* **2016**, *18*, 14177.

[15] R. Dawson, A. I. Cooper, D. J. Adams, *Polym. Int.* **2013**, *62*, 345.

[16] K. Sumida, D. Rogow, J. A. Mason, T. M. McDonald, E. D. Bloch, Z. R. Herm, T. H. Bae, J. R. Long, *Chem. Rev.* **2012**, *112*, 724.

[17] A. Torrisi, R. G. Bell, C. Mellot-Draznieks, *Cryst. Growth Des.* **2010**, *10*, 2839.

[18] Q. Bricaud, A. Cravino, P. Leriche, J. Roncali, *Synth. Met.* **2009**, *159*, 2534.

[19] a) J. Schmidt, M. Werner, A. Thomas, *Macromolecules* **2009**, *42*, 4426; b) W. Lu, D. Yuan, J. Sculley, D. Zhao, R. Krishna, H.C Zhou, *J. Am. Chem. Soc.* **2011**, *133*, 18126.

[20] M. Trunk, A. Herrmann, H. Bildirir, A. Yassin, J. Schmidt, A. Thomas, *Chem. Eur. J.* **2016**, *22*, 7179.

[21] A. Uptmoor, J. Freudenberg, T. Schwäbel, F. Paulus, F. Rominger, F. Hinkel, U. Bunz, *Angew. Chem. Int. Ed.* **2015**, *54*, 14673. [22] A. L. Myers, J. M. Prausnitz, *AIChE J.* **1965**, *11*, 121.

[23] D. Thirion, J. S. Lee, E. Özdemir, C. T. Yavuz, Beilstein, *J. Org. Chem.* **2016**, *12*, 2274.

[24] Y. Lim, I. Choi, H. Lee, I. W. Kim, J. Y. Chang, *J. Mater. Chem. C* **2014**, *2*, 5963.

[25] a) A. Yassin, P. Leriche, J. Roncali, *Macromol. Rapid Commun.* **2010**, *31*, 1467; b) A. Yassin, R. Mallet, P. Leriche, J. Roncali, *ChemElectroChem* **2014**, *1*, 1219; c) A. Yassin, D. Demeter,

J. Roncali, *Tetrahedron Lett.* **2016**, *57*, 3945.

[26] Y. Zhao, X. Liu, Y. Han, *RSC Adv.* **2015**, *5*, 30310.

[27] A. Kumar, D. G. Madden, M. Lusi, K. J. Chen, E. Daniels,

T. Curtin, J. Perry, M. Zaworotko, *Angew. Chem. Int. Ed.* **2015**, *54*, 14372.

[28] a) HOOMD-Blue Web page, http://codeblue.umich.edu/hoomdblue (accessed April 2016); b) T. D. Nguyen, C. L. Phillips, J. A. Anderson, S. C. Glotzer, *Comput. Phys. Commun.* **2011**, *182*, 2307; c) I. T. Todorov, W. Smith, K. Trachenko, M. T. Dove, *J. Mater. Chem.* **2006**, *16*, 1911.

[29] a) J. X. Jiang, F. Su, A. Trewin, C. D. Wood, H. Niu, J. T. A. Jones,

Y. Z. Khimyak, A. I. Cooper, *J. Am. Chem. Soc.* **2008**, *130*, 7710; b) J. Jiang, F. Su, A. Trewin, C. D. Wood, N. L. Campbell, H. Niu, C. Dickinson, A. Y. Ganin, M. J. Rosseinsky, Y. Z. Khimyak, A. I. Cooper, *Angew. Chem. Int. Ed.* **2007**, *46*, 1; c) A. Trewin,

D. J. Willock, A. I. Cooper, *J. Phys. Chem. C* **2008**, *112*, 20549. [30] C. Xu, N. Hedin, *Mater. Today* **2014**, *17*, 397.